

Kinetics of hydrogen-transfer isomerizations of butoxyl radicals†

Jingjing Zheng and Donald G. Truhlar*

Received 5th January 2010, Accepted 21st April 2010

First published as an Advance Article on the web 25th May 2010

DOI: 10.1039/b927504e

Five isomerization reactions involving intramolecular hydrogen-transfer in butoxyl radicals have been studied using variational transition state theory with small curvature tunneling. A set of best estimates of barrier heights and reaction energies for these five reactions was obtained by using coupled cluster theory including single and double excitations with a quasiperturbative treatment of connected triple excitations and a basis set extrapolated to the complete basis set limit plus core–valence correlation contributions and scalar relativistic corrections. This work predicts high-pressure limiting rate constants of these five reactions over the temperature range 200–2500 K and clarifies the available experimental data from indirect measurements. This study shows the importance of performing rate calculations with proper accounting for tunneling and torsional anharmonicity. We also proposed two new models for use in fitting rate constants over wide ranges of temperature.

1. Introduction

Butanol derived from biomass, typically 1-butanol, has been proposed as an alternative to conventional fossil fuels for transportation. 1-Butanol has some advantages over ethanol, which is the current most widely used fuel, as an additive to gasoline or as a fuel in its own right. The advantages include lower vapor pressure, higher energy density, ability to be blended at higher concentrations, and high tolerance to water contamination. It has been shown that butanol can be used as a direct replacement for gasoline in spark ignition engines with few or no modifications,¹ and it is also under consideration as a blending compound in diesel fuels.

Because of butanol's potential advantages as a fuel, it is an important goal to develop kinetic and mechanistic models of its combustion.^{2–6} Butoxyl radicals are intermediates in the combustion of butanol, and they can dissociate, isomerize, or react with other molecules or radicals. Intramolecular hydrogen-transfer isomerization reactions compete with decompositions, and understanding the kinetics of butoxyl radicals is important for modeling the combustion of butanol. Some experimental⁷ and theoretical⁸ studies show that the activation energy of 1-butoxyl radical for isomerization is lower than that for decomposition.

The previous theoretical studies^{8–10} took the values calculated by the BAC-MP4,¹¹ G2,¹² and G3¹³ electronic structure model chemistries as the best estimates of barrier heights for butoxyl isomerization and used them to validate density functional theory¹⁴ (DFT) calculations. However G2 and G3 have been shown to give errors similar to those of some modern density functionals for barrier height calculations.¹⁵ The rapid

development of computational facilities and theoretical methods make it possible to perform benchmark calculations using coupled cluster theory with single and double excitations and a quasiperturbative treatment of connected triple excitations, denoted as CCSD(T),¹⁶ and to extrapolate to the complete basis set (CBS) limit¹⁷ and to run direct dynamics calculations^{18–25} using more accurate density functionals validated against these benchmarks. We take that approach here.

The experimental isomerization rate constants of butoxyl radical have always been derived from the ratio of rate constants for the isomerization reaction of interest and another reaction because it is difficult to measure the reaction rates of the alkoxy radicals directly.^{7,26} For example, Heiss and Sahetchian⁷ measured the ratio of isomerization rate to decomposition rate of 1-butoxyl radical and derived the isomerization rate from this ratio and the known decomposition rate. This indirect measurement can introduce large uncertainty into the derived isomerization. These experimental data only cover narrow range of temperatures, *e.g.* 300–500 K. Theoretical modeling provides an alternative way to clarify these experimental rate constants and make further predictions.

In the present work, we studied the kinetics of the five butoxyl isomerization reactions shown in Scheme 1. First, a set of CCSD(T)/CBS benchmark including core–valence correlation contributions and scalar relativistic corrections is carried out to predict accurate barrier heights and reaction energies for R1–R5. Then these calculations are used to select approximate density functional approximations for each reaction, and density functional methods are used for direct dynamics calculations of reaction rates by variational transition state theory^{27–31} (VTST) with the small-curvature tunneling^{23,31,32} (SCT) approximation.

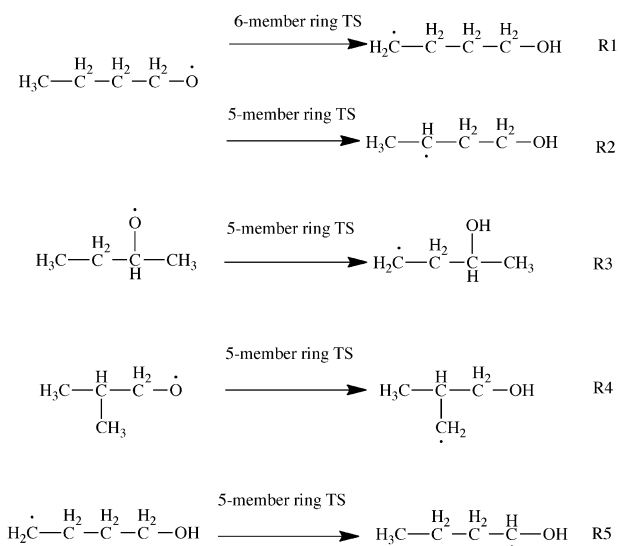
2. Computational details

2.1 Benchmark data

To obtain a set of best estimates of barrier heights and reaction energies for these five reactions, coupled cluster

Department of Chemistry and Supercomputing Institute, University of Minnesota, Minneapolis, Minnesota 55455-0431, USA. E-mail: truhlar@umn.edu

† Electronic supplementary information (ESI) available: Cartesian coordinates of the optimized geometries by M06-2X/MG3S method and the methods specified in Table 2 of the text and the calculated rate constants in tabular form. See DOI: 10.1039/b927504e



Scheme 1

theory including single and double excitations with a quasiperturbative treatment of connected triple excitations, CCSD(T), was employed with a basis set extrapolated to the complete basis set (CBS) limit. The CBS limit was estimated with a set of augmented correlation consistent basis sets, aug-cc-pVnZ^{33,34} ($n = D, T, \text{ and } Q$) and using Peterson *et al.*'s extrapolation scheme.¹⁷ The CCSD(T)/CBS calculations were based on the frozen core (FC) approximation. Then the core–valence (CV) correlation contributions were evaluated by taking the difference between FC and all-electrons CCSD(T) calculations using the MTvtz^{35,36} (sometimes denoted as MT in the literature) basis set. Scalar relativistic corrections were calculated as expectation values of the first-order Darwin and mass–velocity terms^{37,38} using the averaged coupled pair functional³⁹ (ACPF) method. The procedures for the core–valence correlation correction and the scalar relativistic correction are taken from the Weizmann-1⁴⁰ method. Geometries were optimized using the M06-2X⁴¹ density functional with the MG3S⁴² (equivalent to 6-311 + G(2df,2p)⁴³ for H, C, and O) basis set. All the CCSD(T) and ACPF calculations were performed by using the *MOLPRO* 2008.1 package.⁴⁴

2.2 Density functional calculations

We tested various combinations of density functionals and basis sets in order to find an affordable method (combination of density functional and basis set) for direct dynamics calculations that has high accuracy as judged by comparison with our best estimates of barrier heights and reaction energies. The tested density functionals are B3LYP,^{45–47} B3LYP,^{45,48,49} BMK,⁵⁰ M05,⁵¹ M05-2X,⁵¹ M06,⁴¹ M06-2X, M08-SO,⁵² MPW1K,⁵³ MPWB1K,^{49,54,55} PWB6K,⁵⁶ and ω B97X-D.^{57,58} The basis sets are 6-31 + G(d,p) (140),⁴³ MG3S (251), MG3SXP (276),⁵² cc-pVTZ + (296),^{33,43,59,60} maug-cc-pVTZ (296),^{33,34,43,59,60} and aug-cc-pVTZ (437),^{33,34,59} where the number in parentheses is the number of contracted basis functions. The geometries used in density functional calculations were optimized at the consistent level, and minima and saddle points were confirmed by frequency analysis.

All the DFT stationary-point calculations were performed using “ultrafine” integration grids except that M08-SO/MG3SXP and ω B97X-D/MG3S calculations for R1, R2, and R5 used grids defined as the keyword *Int(Grid = -96032)* in the *Gaussian* program. The keyword *Int(Grid = -96032)* requests 96 radial shells around each atom, and a spherical product grid having 32 θ points and 64 ϕ points in each shell. The reason to use such grids (even finer than ultrafine) is that ultrafine integration grids gave imaginary frequencies for the reactant and/or product of R1 when using M08-SO/MG3SXP and ω B97X-D/MG3S. All density functional calculations were carried out using the *Gaussian* 03 package,⁶¹ the *MN-GFM 4.1* module,⁶² and the *Gaussian* 09 package.⁶³ Note that all the DFT rate calculations used *ultrafine* integration grids in the direct dynamics calculations except the calculations for the reactant of R5 used the grids defined as *Int(Grid = -96032)* in Gaussian program. The reason to use such finer grids for this reactant is that *ultrafine* integration grids give quite different frequencies for some low-frequency modes than the finer grids. For example, M08-SO/6-31 + G(d,p) gave 73 cm⁻¹ for the CH₂ group torsion frequency using the finer grids; however the ultrafine grids gave 123 cm⁻¹ for this mode. Since the calculations using the finer grids should give more precise results, we adopt these frequencies for the reactant of reaction R5 in the rate calculations. We also checked the frequencies of other stationary points in the reactions R1–R5 calculated by both integration grids, which only differ by a few wavenumbers.

2.3 Torsions

Since torsions are very anharmonic, the hindered-rotor^{64–66} approximation was used to account for anharmonicity in some of the torsion modes. We first considered using this treatment for reaction R5 to see how various treatments of vibrations, *e.g.* harmonic oscillator or hindered rotor, change the rate constants. Various schemes for treating torsions have been tested and discussed extensively in a previous study.⁶⁷

The method for treating the hindered rotor in this work is called the *C ω* scheme,^{68–70} which is the recommended method in ref. 67 when only the geometries and frequencies are known. In this scheme, the moment of inertia for the minimum-energy point of the internal rotation potential curve is calculated by a curvilinear (*C*) model,⁶⁵ harmonic-oscillator frequencies are obtained by electronic structure calculations, and the barrier of internal rotation is calculated by eqn (18) of ref. 68.

Since the vibrational partition function is very sensitive to the low frequencies, we list the five lowest harmonic vibrational frequencies of the reactants and saddle points of R1–R5 in Table 1. The CH₂ and OH torsion modes of the reactant of R5 are unique in that they do not occur in the reactants of R1–R4. Two torsion modes involving the CH₂ (mode 36 in Table 1) and OH (mode 32 in Table 1) groups of the reactant and one torsion mode involving OH group (mode 33 in Table 1) in the generalized transition state of R5 were treated with the *C ω* scheme. For mode 36 in the reactant, we treated CH₂ as one rotating group and the rest of the molecule as the other rotating group in the torsion. For mode 32 in the reactant and mode 33 in the generalized transition states, we

Table 1 The lowest five vibrational frequencies for R1–R5 (unit: cm^{-1}) calculated by the M08-SO density functional^a

| Mode | R1 | R2 | R3 | R4 | R5 |
|--------------|------------------|------------------|------------------|------------------|------------------|
| Reactant | | | | | |
| 32 | 379 | 381 | 339 | 339 | 264 ^b |
| 33 | 241 ^b | 242 ^b | 237 ^b | 251 | 183 |
| 34 | 176 | 179 | 218 ^b | 240 ^b | 116 ^b |
| 35 | 111 ^b | 108 ^b | 213 | 219 ^b | 112 |
| 36 | 102 | 103 | 110 | 105 | 73 ^b |
| Saddle point | | | | | |
| 31 | 483 | 601 | 466 | 429 ^b | 480 |
| 32 | 446 | 345 | 404 ^b | 391 | 398 |
| 33 | 398 ^b | 211 ^b | 308 | 296 | 335 ^b |
| 34 | 304 | 205 | 219 ^b | 215 ^b | 183 |
| 35 | 155 | 147 | 149 | 163 | 143 |

^a The basis sets are indicated in Table 2. The frequencies were calculated by the GAUSSIAN 03 program and the MN-GFM 4.3 module and are presented here without scaling although they are scaled (see Table 6) for dynamics calculations. The integration grids defined by the *Int(Ultrafine)* keyword were used for all calculations except for the reactant of reaction R5, for which we used the *Int(Grid = -96032)* keyword. ^b Torsion mode.

treated OH as one group and the rest of the system as the other group. Mode 34 of the reactant of R5 in Table 1 is a complicated motion involving two torsions, that is, simultaneous torsions by the CH_2 group and the HOCH_2 group. Since no validated method is currently available to treat this kind of complicated torsion motion accurately, we used the harmonic-oscillator approximation for this mode. Fig. 1 plots the ratio of rate constants calculated by the hindered-rotor

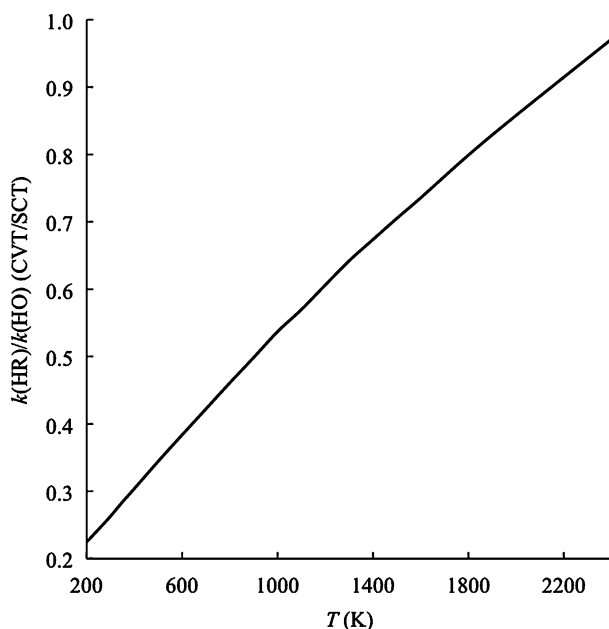


Fig. 1 The ratio of rate constant calculated by the hinder-rotor approximation for selected torsion modes of R5 to the rate constant calculated with the harmonic-oscillator approximation. The calculations are carried out using CVT/SCT with the M08-SO/6-31+G(d,p) density functional approximation. The modes treated as hindered rotors are modes 32 and 36 of the reactant and mode 33 of the generalized transition states. The other vibrational modes in both calculations were treated as harmonic oscillators.

approximation and the harmonic-oscillator approximation at the level of canonical variational theory^{27–29,31} with the small curvature tunneling approximation^{23,30–32} (CVT/SCT) for reaction R5. For this particular reaction, the HO approximation overestimates rate constants at low temperatures and underestimates rate constants at high temperatures as compared to the rate constants calculated using HR approximation for the selected torsion modes. But these two approximations only lead to differences of rate constants by a factor of 0.6–1.2. For intermediate temperatures, e.g. 1000 K, the HO approximation gives almost same rate as HR because of error cancellation between the partition functions of the transition state and reactant.

As shown in Table 1, reactions R1–R4 also have torsions in reactants and saddle points. But many of them are complicated motions involving more than one torsion or mixtures of torsion and bending. By treating mode 33 (CH_3 group torsion) of reactant in R1 as hindered rotor, the rate is raised by 2% at 1000 K and by 13% at 2400 K. Similar small effect are found for other modes (except for the three modes of R5 discussed above). Therefore in the rate calculations in this work, the vibrations in reactions R1–R4 are always treated by the harmonic-oscillator approximation; two torsion modes (mode 32 and 36) of reactant in R5 and one torsion mode (mode 33) of generalized transition states in R5 are treated as hindered rotors, and the other vibrations in R5 are treated by the harmonic-oscillator approximation.

2.4 Dynamics calculations

The high-pressure-limit rate constants k were calculated by canonical variational theory^{27–29,31} with the small curvature tunneling approximation.^{23,30–32} To make direct dynamics calculations practical for the large butoxy isomers, the calculations were carried out using interpolated variational transition state theory by mapping⁷¹ (IVTST-M). The IVTST-M method involves electronic structure calculations of only a subset of the needed information and generates the rest by a specialized spline-under-tension algorithm. The potential energy, the determinant of the moment of inertia tensor, the generalized-normal-mode vibrational frequencies, and the small-curvature effective reduced mass at any point of the reaction path are obtained by interpolating the input data of the stationary points (reactant, product, and saddle point) geometries and Hessians, H nonstationary Hessians, and G geometries and nonzero gradients. We use the notation IVTST-M- H/G to denote using G geometries, energies, and gradients and H Hessians for nonstationary points in the interpolation, and we assume that there will be at least one gradient point beyond the farthest Hessian point in each direction in order to estimate the curvature components of the reaction path at the farthest out Hessian points by central differences of the gradient. The first step in an IVTST-M calculation is a straight direct dynamics calculation over a limited range of the reaction coordinate to generate the data used in the interpolation stage of the IVTST-M calculation. Here, the straight direct dynamics calculation involved a small range of the reaction path with the reaction coordinate s from -0.50 to 0.50 Å (where distances are scaled to a reduced mass of 1 amu) by

using the Page–McIver integrator⁷² with a step size 0.005 Å. A Hessian matrix was calculated every 9 steps. Hence, each straight direct dynamics calculation generated 202 nonstationary points along the minimum energy path (MEP) with Hessian matrices calculated for 22 of them for the input of IVTST-M calculations. Therefore the full direct dynamics calculations are denoted as IVTST-M-22/202.

The next step in the IVTST-M calculations is to interpolate V_{MEP} (the potential energy along the minimum-energy path) between the reactant and the closest nonstationary point in the reactant channel and between the product and the last energy point in the product channel. For this purpose we first add ten extra points in each of these intervals, and then the combined set of original points (discussed in the previous paragraph) and these 20 extra points are fit to a spline under tension in the mapping variable z defined in eqn (1) of Corchado *et al.*⁷¹ Note that z is signed distance s along the mass-scaled minimum-energy path. The 10 extra points on each side can be evenly spaced in s or evenly spaced in z . In either case, the 10 extra point energies are calculated using a cubic polynomial fitted to $V_{\text{MEP}}(s)$ or $V_{\text{MEP}}(z)$ at three points (the two closest nonstationary points plus reactant or product) and using the fact that energy gradient at reactant or product is zero. For these particular reactions, we found that the cubic polynomial fitting is more stable and physically meaningful when using the variable z than when using the variable s .

We used redundant curvilinear internal coordinates^{73,74} and the harmonic-oscillator (HO) approximation for generalized normal mode analyses for stationary and nonstationary points except that the hindered-rotor (HR) approximation was also used to treat the selected torsion modes in R5 as discussed above. The treatment of torsion modes is discussed in Section 2.3.

The frequency scaling factors for the M08-SO functional with 6-31+G(d,p), MG3S, and cc-pVTZ+ basis sets were optimized by minimizing the root-mean-square errors to reproduce the zero-point-vibrational energies in the ZPVE13/99 database.^{75,76} The optimized scaling factors of the M08-SO density functional are listed in Table 2.

The reaction rate calculations were performed by the *GAUSSRATE* program⁷⁷ interfacing the *POLYRATE* program⁷⁸ and the *Gaussian* 03 electronic structure package⁶¹ and the *MN-GFM* module.⁶²

2.5 Activation energies

The Arrhenius activation energy at temperature T_0 is defined as⁷⁹

$$E_a = -R \left. \frac{d \ln k}{d(1/T)} \right|_{T=T_0} \quad (1)$$

Table 2 The methods used for dynamics calculations and their corresponding frequency scaling factors

| Method | Frequency scaling factor | Used for these reactions |
|--------------------|--------------------------|--------------------------|
| M08-SO/MG3S | 0.9851 | R1 |
| M08-SO/6-31+G(d,p) | 0.9815 | R2, R3, R5 |
| M08-SO/cc-pVTZ+ | 0.9847 | R4 |

where R is the gas constant. In practice the derivative is evaluated by a finite difference approximation using rate constants at $T = T_0 \pm 5$ K.

2.6 Fitting rate constants

It is useful to represent the temperature-dependent rate constants $k(T)$ by parameterized functions $k_M(p_1, \dots, p_N, T)$, with $N = 3$ or 4, where p_1, \dots, p_N are parameters. The parameters were determined by minimizing the root-mean-square residual (RMSR) defined by

$$\text{RMSR} = \left\{ \frac{1}{21} \sum_{i=1}^{21} \left[\ln \frac{k(T_i)}{k_M(p_1, \dots, p_N, T_i)} \right]^2 \right\}^{1/2} \quad (2)$$

where the T_i are 21 temperatures equally spaced in $1/T$ from $T_1 = 200$ K to $T_{21} = 2500$ K.

3. Results and discussion

3.1 Barrier heights

The calculated barrier heights and reaction energies using various methods for reactions R1–R5 are presented in Tables 3–7, respectively. The best estimated barrier heights and reaction energies are calculated by the CCSD(T)/CBS method plus (as discussed in Section 2.1) a core–valence correlation contribution and a scalar relativistic correction; the relative energies of the stationary species in reactions R1–R5 are plotted in Fig. 2. These benchmark calculations show that R1 has a significantly lower barrier height than the other reactions; this is due to the less constrained geometry of the six-member ring transition state for this reaction as compared to a five-member ring transition state for the other reactions. Reactions R2–R5 all go through five-member ring transition states, but they have slightly different barrier heights. The comparison between the forward barrier heights of R2 and R5 indicates that the hydrogen transfer from carbon to oxygen is more favorable in energetics by about 3 kcal mol^{−1} than hydrogen transfer between two carbon sites. The reactions R3 and R4 have very similar barrier heights and reaction energies. The forward barrier heights of R3 and R4 are higher than that of R2 by 1.7 kcal mol^{−1}.

Among the tested density functionals, M08-SO (with various basis sets) predicts the most accurate barrier heights and reaction energies for all five reactions according to the mean unsigned error (MUE) of forward and reverse barrier heights and reaction energy of each reaction. Therefore the M08-SO density functional combined with the basis set that has the lowest MUE (except R3) for a particular reaction was selected for the dynamics calculations. These methods along with the corresponding frequency scaling factors are listed in Table 2. For reaction R3, although the M08-SO/aug-cc-pVTZ method gives the lowest MUE (0.57 kcal mol^{−1}) among the tested density functional methods, M08-SO/6-31+G(d,p) is chosen for dynamics calculation for R3 because it has only slightly higher MUE (0.60 kcal mol^{−1}) but it is much more computationally efficient for the dynamics calculations for such a large system. For a reaction with the size of butoxy radical, dispersion-like interactions within the molecule might be important as shown in a recent study by Gruzman *et al.*⁸⁰ The M08-SO density functional without empirical dispersion

Table 3 Calculated barrier heights and reaction energies (in kcal mol⁻¹) for R1^a

| Method | V_f^\ddagger | V_r^\ddagger | ΔE | MUE |
|--------------------------------------|----------------|----------------|------------|------|
| CCSD(T)/CBS + CV + Rel.//M06-2X/MG3S | 11.89 | 15.79 | -3.90 | 0.00 |
| CCSD(T)/CBS//M06-2X/MG3S | 11.80 | 15.80 | -4.01 | 0.07 |
| M08-SO/MG3S | 12.15 | 15.92 | -3.77 | 0.18 |
| M08-SO/MG3SXP | 12.20 | 15.97 | -3.77 | 0.21 |
| CCSD(T)/aug-cc-pVQZ//M06-2X/MG3S | 11.85 | 15.46 | -3.60 | 0.22 |
| M08-SO/aug-cc-pVTZ | 12.25 | 15.80 | -3.56 | 0.24 |
| M08-SO/cc-pVTZ + | 12.25 | 15.73 | -3.48 | 0.28 |
| M06-2X/maug-cc-pVTZ | 12.12 | 15.20 | -3.09 | 0.54 |
| M08-HX/cc-pVTZ + | 12.71 | 15.92 | -3.21 | 0.55 |
| CCSD(T)/aug-cc-pVTZ//M06-2X/MG3S | 11.95 | 14.94 | -2.98 | 0.61 |
| M05-2X/MG3SXP | 11.91 | 14.85 | -2.94 | 0.64 |
| M05-2X/cc-pVTZ + | 11.62 | 14.80 | -3.17 | 0.66 |
| M05-2X/MG3S | 11.98 | 14.81 | -2.83 | 0.71 |
| M08-SO/6-31 + G(d,p) | 12.29 | 15.05 | -2.76 | 0.76 |
| M06-2X/MG3S | 12.53 | 15.24 | -2.72 | 0.79 |
| M06/MG3S | 12.64 | 15.32 | -2.68 | 0.81 |
| CCSD(T)/aug-cc-pVDZ//M06-2X/MG3S | 12.24 | 14.77 | -2.52 | 0.92 |
| M05/MG3S | 14.57 | 17.01 | -2.44 | 1.79 |
| ω B97X-D/MG3S | 12.49 | 13.41 | -0.92 | 1.98 |
| MPW1K/MG3S | 14.56 | 15.30 | -0.74 | 2.11 |
| BMK/MG3S | 13.44 | 13.66 | -0.22 | 2.46 |
| B3LYP/MG3S | 11.43 | 12.05 | -0.61 | 2.49 |
| MPWB1K/MG3S | 13.65 | 13.66 | -0.01 | 2.60 |
| BB1K/MG3S | 13.54 | 13.52 | 0.03 | 2.62 |
| PWB6K/MG3S | 14.69 | 14.47 | 0.22 | 2.75 |

^a Subscript “f” denotes forward and “r” denotes reverse.**Table 4** Calculated barrier heights and reaction energies (in kcal mol⁻¹) for R2^a

| Method | V_f^\ddagger | V_r^\ddagger | ΔE | MUE |
|--------------------------------------|----------------|----------------|------------|------|
| CCSD(T)/CBS + CV + Rel.//M06-2X/MG3S | 19.75 | 26.58 | -6.83 | 0.00 |
| CCSD(T)/CBS//M06-2X/MG3S | 19.64 | 26.53 | -6.89 | 0.07 |
| CCSD(T)/aug-cc-pVQZ//M06-2X/MG3S | 19.70 | 26.10 | -6.40 | 0.32 |
| M08-SO/6-31 + G(d,p) | 20.31 | 26.69 | -6.38 | 0.38 |
| M08-SO/aug-cc-pVTZ | 20.17 | 27.32 | -7.15 | 0.49 |
| M08-SO/cc-pVTZ + | 20.32 | 27.36 | -7.03 | 0.52 |
| M05-2X/cc-pVTZ + | 20.54 | 26.91 | -6.37 | 0.53 |
| M06/MG3S | 20.72 | 27.59 | -6.87 | 0.67 |
| M08-SO/MG3SXP | 20.28 | 27.60 | -7.33 | 0.68 |
| M05-2X/MG3SXP | 20.80 | 26.91 | -6.11 | 0.70 |
| M08-SO/MG3S | 20.32 | 27.63 | -7.31 | 0.70 |
| M06-2X/maug-cc-pVTZ | 20.87 | 27.27 | -6.40 | 0.75 |
| M05-2X/MG3S | 20.91 | 27.01 | -6.10 | 0.77 |
| CCSD(T)/aug-cc-pVTZ//M06-2X/MG3S | 19.81 | 25.45 | -5.65 | 0.79 |
| ω B97X-D/MG3S | 20.68 | 25.26 | -7.33 | 0.92 |
| M08-HX/cc-pVTZ + | 21.21 | 27.55 | -6.34 | 0.98 |
| M06-2X/MG3S | 21.35 | 27.42 | -6.07 | 1.07 |
| CCSD(T)/aug-cc-pVDZ//M06-2X/MG3S | 20.11 | 24.98 | -4.87 | 1.31 |
| B3LYP/MG3S | 19.83 | 24.48 | -4.65 | 1.46 |
| BB1K/MG3S | 21.26 | 25.11 | -3.85 | 1.99 |
| MPWB1K/MG3S | 21.43 | 25.26 | -3.83 | 2.00 |
| MPW1K/MG3S | 22.78 | 27.19 | -4.41 | 2.02 |
| M05/MG3S | 22.64 | 29.70 | -7.06 | 2.08 |
| BMK/MG3S | 21.66 | 25.31 | -3.66 | 2.12 |
| PWB6K/MG3S | 22.47 | 26.00 | -3.53 | 2.20 |

^a Subscript “f” denotes forward and “r” denotes reverse.

corrections outperforms the ω B97X-D functional in which the B97-1 functional was refitted by including long-range exchange corrections and empirical dispersion corrections.

3.2 Torsional anharmonicity

Fig. 3 shows that the calculated CVT/SCT rate constants of R5 over wide range of temperatures are about an order of

magnitude lower than those of R3 and R4 although their barrier height differences are smaller than 0.83 kcal mol⁻¹. This large difference is not caused by tunneling because the SCT transmission coefficients for R3–R5 are close to each other as shown in Fig. 4. And, as discussed in Section 2.3, the large difference is not caused by anharmonicity. To provide insight into the factors that control this aspect of the

Table 5 Calculated barrier heights and reaction energies (in kcal mol⁻¹) for R3^a

| Method | V_f^\ddagger | V_r^\ddagger | ΔE | MUE |
|--------------------------------------|----------------|----------------|------------|------|
| CCSD(T)/CBS + CV + Rel.//M06-2X/MG3S | 21.45 | 25.88 | -4.43 | 0.00 |
| CCSD(T)/CBS//M06-2X/MG3S | 21.36 | 25.85 | -4.49 | 0.06 |
| CCSD(T)/aug-cc-pVQZ//M06-2X/MG3S | 21.45 | 25.52 | -4.07 | 0.24 |
| M08-SO/aug-cc-pVTZ | 22.30 | 26.53 | -4.23 | 0.57 |
| M08-SO/6-31 + G(d,p) | 22.35 | 25.93 | -3.58 | 0.60 |
| M08-SO/cc-pVTZ + | 22.37 | 26.61 | -4.24 | 0.61 |
| M05-2X/cc-pVTZ + | 22.40 | 26.09 | -3.69 | 0.64 |
| CCSD(T)/aug-cc-pVTZ//M06-2X/MG3S | 21.61 | 25.02 | -3.41 | 0.68 |
| M08-SO/MG3SXP | 22.47 | 26.96 | -4.49 | 0.72 |
| M08-SO/MG3S | 22.44 | 26.99 | -4.54 | 0.74 |
| ω B97X-D/MG3S | 22.21 | 24.13 | -4.49 | 0.86 |
| M06-2X/maug-cc-pVTZ | 22.78 | 26.60 | -3.82 | 0.89 |
| M08-HX/cc-pVTZ + | 22.80 | 27.15 | -4.35 | 0.90 |
| M06/MG3S | 22.80 | 26.64 | -3.83 | 0.90 |
| M05-2X/MG3SXP | 22.82 | 26.27 | -3.44 | 0.92 |
| M05-2X/MG3S | 22.90 | 26.27 | -3.36 | 0.97 |
| CCSD(T)/aug-cc-pVDZ//M06-2X/MG3S | 21.90 | 24.86 | -2.96 | 0.98 |
| M06-2X/MG3S | 23.34 | 26.80 | -3.46 | 1.26 |
| M05/MG3S | 24.07 | 27.31 | -3.23 | 1.75 |
| MPW1K/MG3S | 23.93 | 25.52 | -1.59 | 1.89 |
| B3LYP/MG3S | 21.20 | 22.52 | -1.31 | 2.24 |
| MPWB1K/MG3S | 22.93 | 23.83 | -0.90 | 2.36 |
| BB1K/MG3S | 22.72 | 23.54 | -0.82 | 2.41 |
| BMK/MG3S | 23.56 | 24.26 | -0.70 | 2.48 |
| PWB6K/MG3S | 23.99 | 24.62 | -0.63 | 2.53 |

^a Subscript “f” denotes forward and “r” denotes reverse.**Table 6** Calculated barrier heights and reaction energies (in kcal mol⁻¹) for R4^a

| Method | V_f^\ddagger | V_r^\ddagger | ΔE | MUE |
|--------------------------------------|----------------|----------------|------------|------|
| CCSD(T)/CBS + CV + Rel.//M06-2X/MG3S | 21.48 | 26.09 | -4.61 | 0.00 |
| CCSD(T)/CBS//M06-2X/MG3S | 21.40 | 26.09 | -4.69 | 0.06 |
| CCSD(T)/aug-cc-pVQZ//M06-2X/MG3S | 21.51 | 25.79 | -4.28 | 0.22 |
| CCSD(T)/aug-cc-pVTZ//M06-2X/MG3S | 21.69 | 25.34 | -3.65 | 0.64 |
| M08-SO/cc-pVTZ + | 22.52 | 26.92 | -4.39 | 0.70 |
| M06-2X/maug-cc-pVTZ | 22.74 | 27.15 | -4.42 | 0.84 |
| CCSD(T)/aug-cc-pVDZ//M06-2X/MG3S | 22.00 | 25.22 | -3.22 | 0.93 |
| M05-2X/cc-pVTZ + | 22.95 | 26.39 | -3.44 | 0.98 |
| M08-SO/aug-cc-pVTZ | 23.27 | 26.86 | -3.59 | 1.19 |
| M08-SO/6-31 + G(d,p) | 23.20 | 26.02 | -2.81 | 1.20 |
| M06-2X/MG3S | 23.29 | 27.31 | -4.02 | 1.21 |
| M08-SO/MG3S | 23.41 | 27.19 | -3.78 | 1.29 |
| M08-SO/MG3SXP | 23.43 | 27.28 | -3.85 | 1.30 |
| M05-2X/MG3SXP | 23.52 | 26.85 | -3.32 | 1.36 |
| M05-2X/MG3S | 23.61 | 26.67 | -3.06 | 1.42 |
| ω B97X-D/MG3S | 23.24 | 24.14 | -3.85 | 1.49 |
| M08-HX/cc-pVTZ + | 24.02 | 27.15 | -3.13 | 1.70 |
| M06/MG3S | 24.20 | 26.83 | -2.63 | 1.82 |
| M05/MG3S | 24.86 | 27.09 | -2.23 | 2.26 |
| BMK/MG3S | 23.45 | 24.46 | -1.00 | 2.40 |
| MPW1K/MG3S | 24.87 | 25.51 | -0.65 | 2.64 |
| B3LYP/MG3S | 21.95 | 22.54 | -0.59 | 2.68 |
| BB1K/MG3S | 23.71 | 23.59 | 0.11 | 3.15 |
| MPWB1K/MG3S | 23.98 | 23.85 | 0.13 | 3.16 |
| PWB6K/MG3S | 25.01 | 24.61 | 0.40 | 3.34 |

^a Subscript “f” denotes forward and “r” denotes reverse.

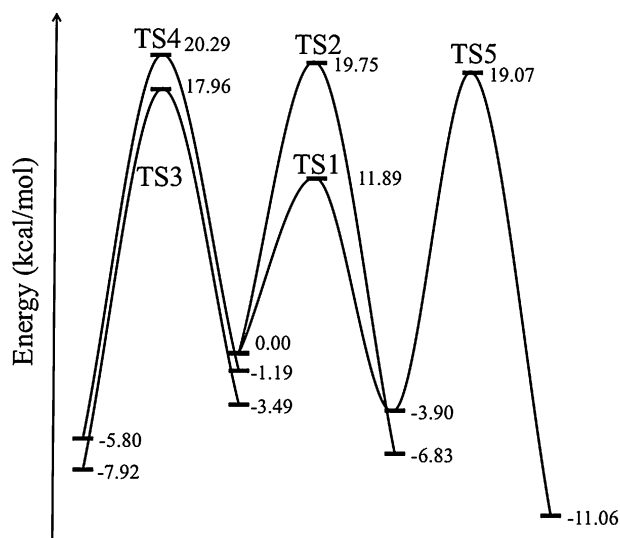
calculated rate constants, the calculated forward barrier heights, free energies of activation, CVT free energies of activation, and vibrational and rotational partition functions for reactants and saddle points are listed in Table 8 for $T = 2000$ K. The partition functions listed in Table 8 were calculated using the rigid-rotor harmonic-oscillator approximation for the first five rows of the table. The temperature 2000 K is

selected to simplify the analysis by avoiding the consideration of tunneling. The large differences of the rate constants are reflected in the differences of free energies of activation, as can be seen in Table 8. The quantity that causes the large difference of activation free energies between R5 and R3 or R4 is that the vibrational partition function of the reactant in R5 is one order of magnitude larger than those of R3 and R4.

Table 7 Calculated barrier heights and reaction energies (in kcal mol⁻¹) for R5^a

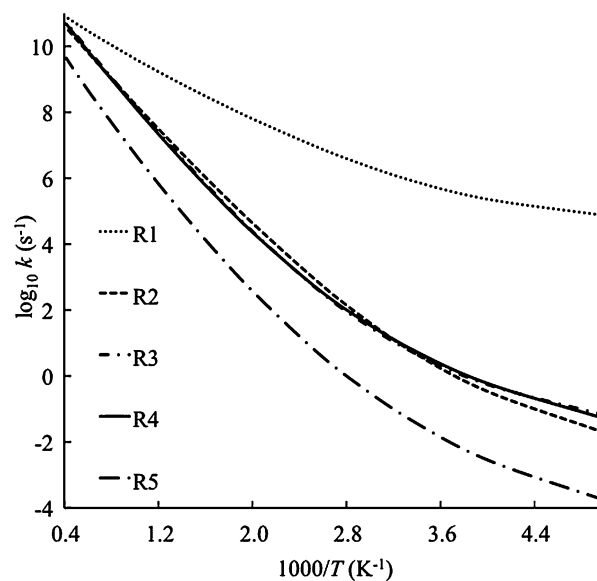
| Method | V_f^\ddagger | V_r^\ddagger | ΔE | MUE |
|----------------------------------|----------------|----------------|------------|------|
| CCSD(T)/CBS+CV+Rel.//M06-2X/MG3S | 22.97 | 30.13 | -7.16 | 0.00 |
| CCSD(T)/CBS//M06-2X/MG3S | 22.89 | 29.96 | -7.06 | 0.12 |
| M08-SO/6-31+G(d,p) | 23.18 | 30.10 | -6.92 | 0.16 |
| CCSD(T)/aug-cc-pVQZ//M06-2X/MG3S | 22.88 | 29.86 | -6.98 | 0.18 |
| CCSD(T)/aug-cc-pVTZ//M06-2X/MG3S | 22.85 | 29.68 | -6.83 | 0.30 |
| M05-2X/MG3S | 23.32 | 30.64 | -7.32 | 0.34 |
| M05-2X/MG3SXP | 23.32 | 30.65 | -7.33 | 0.34 |
| M06/MG3S | 22.44 | 29.87 | -7.43 | 0.36 |
| M08-SO/MG3S | 23.34 | 30.69 | -7.35 | 0.37 |
| M05-2X/cc-VTZ+ | 23.57 | 30.75 | -7.18 | 0.41 |
| M06-2X/MG3S | 23.31 | 30.75 | -7.44 | 0.41 |
| M06-2X/maug-cc-pVTZ | 23.44 | 30.77 | -7.33 | 0.42 |
| M08-SO/MG3SXP | 23.34 | 30.81 | -7.46 | 0.45 |
| M08-SO/cc-VTZ+ | 23.39 | 30.82 | -7.43 | 0.46 |
| M08-HX/cc-VTZ+ | 23.23 | 30.82 | -7.59 | 0.46 |
| MPW1K/MG3S | 23.31 | 30.86 | -7.55 | 0.49 |
| M08-SO/aug-cc-pVTZ | 23.42 | 30.88 | -7.46 | 0.50 |
| PWB6K/MG3S | 22.57 | 30.73 | -8.17 | 0.67 |
| B3LYP/MG3S | 21.96 | 30.12 | -8.16 | 0.68 |
| ω B97X-D/MG3S | 21.85 | 30.06 | -8.21 | 0.75 |
| BMK/MG3S | 22.00 | 30.33 | -8.33 | 0.78 |
| CCSD(T)/aug-cc-pVDZ//M06-2X/MG3S | 22.68 | 28.79 | -6.10 | 0.90 |
| MPWB1K/MG3S | 21.61 | 29.95 | -8.34 | 0.91 |
| BB1K/MG3S | 21.51 | 29.90 | -8.39 | 0.98 |
| M05/MG3S | 24.41 | 31.97 | -7.56 | 1.23 |

^a Subscript “f” denotes forward and “r” denotes reverse.

**Fig. 2** Energy landscape of R1–R5 calculated by CCSD(T)/CBS with core–valence correlation corrections and scalar relativistic corrections.

The reactants of R3 and R4 only have one vibrational mode with frequency lower than 200 cm⁻¹. However, the reactant of R5 has 4 vibrational modes with frequencies lower than 200 cm⁻¹. The existence of more low-frequency vibrational modes in the reactant of R5 leads to a significantly larger vibrational partition function and then eventually to much lower reaction rate constants. The difference of the number of low vibrational frequencies between R5 and R3 or R4 is due to their structural difference, rather than to the particular theoretical method used for frequency calculations.

To illustrate the uncertainty of the calculated frequencies due to theoretical methods, we list the calculated torsion-mode

**Fig. 3** The plots of calculated CVT/SCT rate constants with rigid-rotor harmonic-oscillator approximation for R1–R4 and selected modes treated as hindered rotors for R5. The M08-SO density functional with basis sets listed in Table 2 was used in the calculations.

frequencies involving the radical site CH₂ group in the reactant of R5 by various methods in Table 9. The calculated torsion frequencies involving the CH₃ group in the reactant of R1 are also given in Table 9 for comparison. The frequency of the CH₂ torsion in the reactant of R5 varies from 24 cm⁻¹ to 123 cm⁻¹. The range of this frequency that is caused by different theoretical methods, *i.e.*, by various combinations of density functional and basis set and different integration grids, corresponds to the changes of the rate constant by a

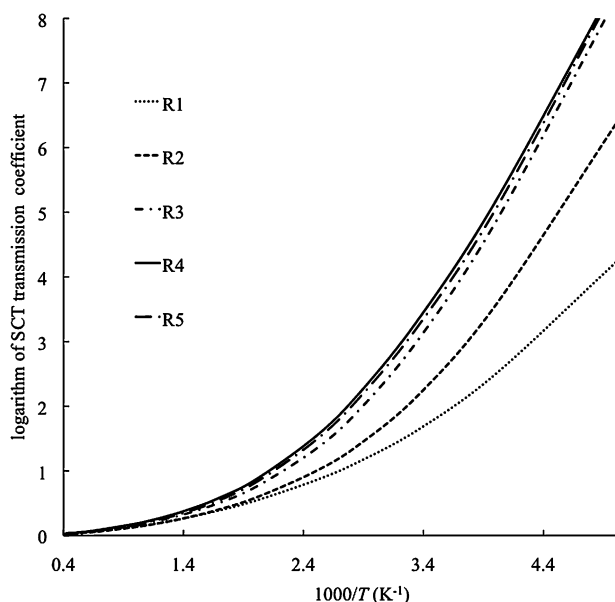


Fig. 4 Logarithm to the base 10 of calculated SCT transmission coefficients of R1–R5 versus reciprocal temperature. The M08-SO density functional with basis sets listed in Table 6 was used in the calculations.

factor of up to 5. These examples show the importance of calculating the low vibrational frequencies accurately. Even when the harmonic frequency is calculated accurately, there is uncertainty due to the neglect of or treatment of anharmonicity.

3.3 Reaction rates

The calculated CVT/SCT reaction rate constants of R1 were plotted in Fig. 5 together with other theoretical¹⁰ and experimental^{7,26} data for $T = 298$ – 500 K. The experimental data by Heiss and Sahetchian⁷ and Cassanelli *et al.*²⁶ were not obtained from direct measurements for R1. Their isomerization rate constants for R1 were derived from the ratio of the rate of R1 to the rate of another reaction. In particular, Heiss *et al.* measured the ratio of rate of the isomerization to that of decomposition of *n*-butoxyl radical, and Cassanelli *et al.* measured the ratio of the isomerization rate of *n*-butoxyl radical to the rate of the reaction between *n*-butoxyl and oxygen molecule. In both studies, an Arrhenius equation

$$k = A \exp(-E_a/RT) \quad (3)$$

Table 8 Comparison of barrier heights (kcal mol⁻¹), maximum of free energy of activation (kcal mol⁻¹) and partition functions (unitless) at $T = 2000$ K for forward reactions R1–R5^a

| | ΔV^\ddagger | ΔG^\ddagger | ΔG^{CVT} | $Q_{\text{rot}}^{\text{R}}$ | $Q_{\text{vib}}^{\text{R}}$ | Q_{rot}^\ddagger | Q_{vib}^\ddagger |
|-----------------|---------------------|---------------------|-------------------------|-----------------------------|-----------------------------|---------------------------|---------------------------|
| R1 | 12.15 | 26.50 | 27.05 | 1.71E+06 | 1.27E+03 | 1.46E+06 | 4.00E+01 |
| R2 | 20.31 | 30.94 | 31.18 | 1.73E+06 | 1.26E+03 | 1.55E+06 | 9.43E+01 |
| R3 | 22.35 | 29.56 | 30.06 | 1.66E+06 | 5.92E+02 | 1.47E+06 | 1.09E+02 |
| R4 | 22.52 | 29.94 | 30.58 | 1.68E+06 | 5.93E+02 | 1.52E+06 | 1.04E+02 |
| R5 | 23.18 | 40.20 | 40.24 | 1.70E+06 | 9.68E+03 | 1.57E+06 | 1.44E+02 |
| R5 ^b | 23.18 | 39.30 | 39.34 | 1.70E+06 | 1.33E+04 | 1.57E+06 | 2.48E+02 |

^a Note that the zero of energy for vibrational partition functions is the equilibrium value of the potential not the zero point level. The superscript R denotes reactant, and the superscript ‡ denotes the saddle point. ^b The hindered-rotor approximation was used for selected torsion modes in this row for reaction R5 (see text).

was used to evaluate the isomerization rate based on the measured ratio and the known rate of the reference reaction. Tunneling, which often causes severe deviations from the simple Arrhenius temperature dependence, may lead to quite large error for the hydrogen-transfer isomerization rate obtained by this procedure at a temperature as low as 300 K. Fig. 5 also shows theoretical rate constants for R1 by Somnitz¹⁰ that are based on Rice–Ramsperger–Kassel–Marcus (RRKM) theory including tunneling (T) contributions calculated based on the assumption of conservation of vibrational energy (CVE, *i.e.* zero-point energies along reaction path are assumed to be constant) and also including a master equation (ME). The CVET transmission coefficient is 2.7 at $T = 300$ K.¹⁰ In the Somnitz study,¹⁰ the tunneling contributions for R1 was also calculated based on the zero curvature tunneling (ZCT) formalism but with the vibrationally adiabatic ground-state potential along the reaction path fitted to an Eckart potential; this ZCT-like transmission coefficient is only 1.4 at $T = 300$ K, but the use of Eckart fits is known⁸¹ to be unreliable. We note though that the ZCT approximation usually underestimates

Table 9 The calculated torsion frequencies in the reactants of R1 and R5 (unit: cm⁻¹)^a

| Method | CH ₂ (R5) | CH ₃ (R1) |
|-----------------------------------|----------------------|----------------------|
| B3LYP/MG3S | 84 | 250 |
| BB1K/MG3S | 83 | 255 |
| BMK/MG3S | 67 | 252 |
| M05-2X/MG3S | 46 | 252 |
| M05-2X/MG3SXP | 45 | 254 |
| M05-2X/cc-pVTZ + | 48 | 251 |
| M05/MG3S | 83 | 249 |
| M06-2X/MG3S | 97 | 253 |
| M06/MG3S | 51 | 252 |
| M08-HX/cc-pVTZ + | 24 | 243 |
| M08-HX/cc-pVTZ + ^b | 68 | 232/253 ^c |
| M08-SO/6-31 + G(d,p) | 123 | 242 |
| M08-SO/6-31 + G(d,p) ^b | 73 | 241 |
| M08-SO/aug-cc-pVTZ | 98 | 239 |
| M08-SO/MG3S | 98 | 241 |
| M08-SO/MG3SXP | 60 | 240 |
| M08-SO/cc-pVTZ + | 84 | 241 |
| MPW1K/MG3S | 88 | 255 |
| MPWB1K/MG3S | 81 | 254 |
| ωB97X-D/MG3S | 65 | 252 |

^a The integration grids defined by *Int(Ultrafine)* were used for all calculations except where indicated otherwise. ^b These calculations used *Int(Grid = -96032)* integration grids. ^c Two modes involve CH₃ group torsion.

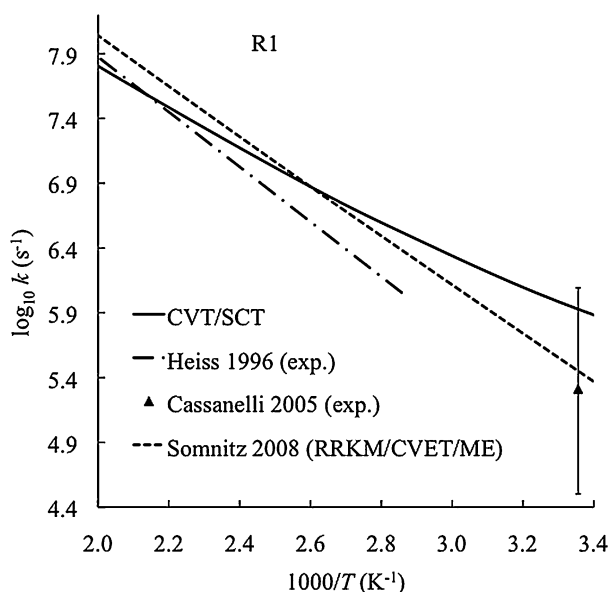


Fig. 5 Calculated rate constants of the forward reaction R1 by CVT/SCT in this work and by the RRKM/CVET/ME method (CVET denotes CVE tunneling and ME denotes master equation) by Somnitz¹⁰ together with experimental data by Heiss and Sahetchian⁷ and by Cassanelli *et al.*²⁶

the tunneling contribution.^{29,82} Our calculations in the present work show that the ZCT transmission coefficient is 5.3 and is smaller than the SCT one (40.9) by a factor 7.7 at $T = 300$ K. Somnitz's RRKM/CVET/ME rate constants agree with Cassanelli *et al.*'s data very well at $T = 298$ K. The agreement between RRKM/CVET/ME data and Cassanelli *et al.*'s data at low temperature is consistent with his rate constants being too large at high temperatures because tunneling is underestimated. We found that the variational effect for this reaction (R1) is significant, with the rate constant ratio of CVT to TST ranging from 0.83 to 0.90.

The calculated forward CVT/SCT rate constants of R1–R5 are plotted in Fig. 3 over the temperature range 200–2400 K. Since R1 has a much lower barrier height than the others, its rate constants are much higher than others as shown in Fig. 3 especially in low temperature region. At high temperature, for instance at $T = 2400$ K, the rate constant of R1 gets very close to those of R2–R4. The barrier height of R2 is about 2 kcal mol⁻¹ lower than those of R3 and R4. A barrier height difference of 2 kcal mol⁻¹ corresponds to rate constants that are different by a factor of 29 at $T = 300$ K if one uses conventional TST with the assumption that the partition functions are the same. The calculated TST rate constant of R2 (see ESI†) at $T = 300$ K is only 6 times larger than R3 and 11 times larger than R4. However, CVT/SCT rate constants of R2 are very close to or even lower than those of R3 and R4 above 300 K, which is because the tunneling contributions in R3 and R4 are larger than those in R2 by factors of 7 and 14, respectively. The calculated logarithms of SCT transmission coefficients are plotted vs. $1000/T$ in Fig. 4 for R1–R5. The relative contribution of tunneling to a reaction can be qualitatively associated with the barrier height and barrier width, and the imaginary frequency at the saddle point is the

simplest single indicator of barrier width (although it is not a perfect indicator because it is associated with the classical barrier, not the vibrationally adiabatic barrier, which is more relevant, and because it is only concerned with the width of the classical barrier near its top). Using these two indicators, one finds that reactions with a higher barrier height and higher imaginary frequency usually have a larger tunneling contribution. R1 has a barrier height that is at least 8 kcal mol⁻¹ lower than that of the other reactions; therefore it has the smallest SCT transmission coefficients. R2 not only has a barrier height that is 2 kcal mol⁻¹ lower than that for reactions R3–R5, but also its imaginary frequency (1643i cm⁻¹) at saddle point is about 200i cm⁻¹ lower than that for R3–R5 (1851i–1986i cm⁻¹), thus the tunneling contribution for R2 is also significantly smaller than those for R3–R5. The SCT transmission coefficients for reactions R3–R5 are very similar to each other, which is correlated with the similar barrier heights and similar imaginary frequencies of these reactions. This discussion of factors affecting tunneling (and hence affecting reaction rates) shows the importance of performing rate calculations at a reliable (validated) level of dynamical theory when analyzing reaction mechanisms; merely estimating rates based on barrier heights may lead to incorrect conclusions.

3.4 Activation energies

Since the Arrhenius plots of the CVT/SCT rate constants are curved in Fig. 3 for all the five reactions, the activation energy computed from the slope of the Arrhenius plot depends on temperature. The calculated activation energies using the CVT/SCT approximation for the five reactions at various temperatures are listed in Table 10. We also list the activation energies using the TST, CVT, and CVT/ZCT approximations for comparison, where TST denotes conventional transition state theory, that is, transition state at the saddle point and a

Table 10 Activation energies (kcal mol⁻¹) for the five reactions at various temperatures^a

| | | 300 K | 400 K | 600 K | 1000 K | 1500 K | 2400 K |
|----|---------|-------|-------|-------|--------|--------|--------|
| R1 | TST | 10.0 | 10.0 | 10.1 | 10.5 | 10.9 | 11.3 |
| | CVT | 10.1 | 10.0 | 10.1 | 10.5 | 10.8 | 11.1 |
| | CVT/ZCT | 7.7 | 8.5 | 9.2 | 9.9 | 10.4 | 10.9 |
| | CVT/SCT | 4.9 | 6.7 | 8.0 | 9.2 | 10.0 | 10.6 |
| R2 | TST | 18.5 | 18.5 | 18.6 | 18.9 | 19.2 | 19.5 |
| | CVT | 18.5 | 18.5 | 18.6 | 18.8 | 19.1 | 19.3 |
| | CVT/ZCT | 14.5 | 16.1 | 17.2 | 18.0 | 18.5 | 18.8 |
| | CVT/SCT | 10.3 | 14.0 | 16.2 | 17.5 | 18.2 | 18.6 |
| R3 | TST | 19.9 | 20.0 | 20.1 | 20.6 | 21.0 | 21.4 |
| | CVT | 20.0 | 20.0 | 20.1 | 20.5 | 20.8 | 21.1 |
| | CVT/ZCT | 13.7 | 16.5 | 18.3 | 19.5 | 20.1 | 20.6 |
| | CVT/SCT | 8.7 | 13.4 | 17.1 | 19.0 | 19.8 | 20.4 |
| R4 | TST | 20.3 | 20.3 | 20.4 | 20.8 | 21.2 | 21.7 |
| | CVT | 20.3 | 20.3 | 20.4 | 20.8 | 21.0 | 21.3 |
| | CVT/ZCT | 13.2 | 16.1 | 18.2 | 19.5 | 20.2 | 20.7 |
| | CVT/SCT | 8.7 | 12.9 | 16.9 | 19.0 | 19.9 | 20.5 |
| R5 | TST | 21.3 | 21.4 | 21.8 | 22.8 | 23.9 | 25.5 |
| | CVT | 21.3 | 21.4 | 21.8 | 22.8 | 23.9 | 25.5 |
| | CVT/ZCT | 13.9 | 16.7 | 19.3 | 21.4 | 23.0 | 24.9 |
| | CVT/SCT | 9.9 | 14.2 | 18.4 | 21.1 | 22.9 | 24.8 |

^a From rate constants with harmonic-oscillator approximation for R1–R4 and hindered-rotor approximation for torsion modes for R5 with other modes treated as harmonic oscillators.

transmission coefficient of unity. Notice that the CVT/SCT activation energies are always the lowest of the four methods, being 0.5–11.6 kcal mol⁻¹ lower than TST and CVT and 0.1–5.0 kcal mol⁻¹ lower than CVT/ZCT. Furthermore, the CVT/SCT energy of activation depends dramatically on temperature, varying by 5.7 to 14.9 kcal mol⁻¹ from 300 K to 2400 K. The variation would be even greater if we considered lower temperatures.

The CVT/SCT rate constants of reactions R1–R5 were first fitted to the popular modified Arrhenius equation,

$$k = A \left(\frac{T}{300 \text{ K}} \right)^n e^{-E/RT} \quad (4)$$

where A , n , and E are fitting parameters, and R is the gas constant. We label this equation as Model 1 here. Model 1 has been very widely used for fitting experimental or theoretical rate constants in the literature. The fitted parameters for reactions R1–R5 are listed in Table 11 along with the root-mean-square residuals of $\ln k$. The table shows that Model 1 gives quite large fitting residuals. The activation energy given by eqn (1) and (4) is

$$E_a = E + nRT \quad (5)$$

In order to understand why eqn (4) provides a poor fit, we refer to Table 10, where the temperatures are spaced approximately evenly in $1/T$, but far from evenly in T . Table 10 shows that E_a is much closer to being a linear function of $1/T$ than it is to being a linear function of T . Motivated by this observation, we propose a new three-parameter formula, called Model 2. The Model 2 rate constant expression and its corresponding activation energy are

$$k = C \exp \left[- \left(D_1 - \frac{D_2}{T} \right) / RT \right], \quad (6)$$

$$E_a = D_1 - \frac{2D_2}{T}, \quad (7)$$

where C , D_1 , and D_2 are fitting parameters ($D_1 > 0$ and $D_2 > 0$), and R is the gas constant. This model gives a much smaller RMSR than Model 1, as shown in Table 11. However, the activation energy doesn't have the correct asymptotic behavior in the low-temperature limit.

Therefore we propose another model with one more parameter to give small fitting error and have the correct low-temperature asymptotic behavior for activation energy and rate constant, which is called Model 3. The Model 3 rate constant expression and its corresponding activation energy are

$$k = A \left(\frac{T}{300} \right)^n \exp \left[- \frac{E(T + T_0)}{R(T^2 + T_0^2)} \right] \quad (8)$$

$$E_a = E \frac{T^4 + 2T_0T^3 - T_0^2T^2}{(T^2 + T_0^2)^2} + nRT \quad (9)$$

where A , n , E , and T_0 are fitting parameters, and R is the gas constant. The fitting results are given in Table 11. This model reduces the fitting error further compared to Model 2 over a wide range of temperature for R2–R5 and has similar error as Model 2 for R1. More importantly, Model 3 gives the correct low-temperature asymptotic behavior for the activation energy, *i.e.* the activation energy becomes 0 at $T = 0$ K, which is the correct limit.^{83,84} To illustrate the discrepancy caused by fitted models, we plot the calculated rate constants (data used in fitting) and the rate constants obtained by the Model 1, Model 2, and Model 3 in Fig. 6 for reaction R2, which is the case for which Model 3 gives the largest RMSR.

Model 3 clearly provides a better representation of the temperature dependence than the popular Model 1. One can only wonder how much unintentional bias has been introduced into representations of experimental data by the almost universal adoption of Model 1. The 3-parameter model, Model 2, can be used when less experimental data are available than needed to

Table 11 The fitted parameters using three modified Arrhenius equations for reactions R1–R5 for temperature from 200 K to 2500 K^a

| Parameter | Reaction | | | | |
|---|------------------------|------------------------|------------------------|------------------------|------------------------|
| | R1 | R2 | R3 | R4 | R5 |
| Model 1 $k = A \left(\frac{T}{300 \text{ K}} \right)^n e^{-E/RT}$ | | | | | |
| A (s ⁻¹) | 1.315×10^8 | 1.241×10^6 | 2.863×10^4 | 4.132×10^4 | 8.237×10^2 |
| n | 3.632 | 6.204 | 8.112 | 7.838 | 8.638 |
| E (kcal mol ⁻¹) | 2.689 | 6.710 | 4.449 | 4.655 | 5.268 |
| RMSR | 0.390 | 0.754 | 0.874 | 0.777 | 0.788 |
| Model 2 $k = C e^{-\left(D_1 - \frac{D_2}{T}\right)/RT}$ | | | | | |
| C (s ⁻¹) | 8.336×10^{11} | 4.317×10^{12} | 8.916×10^{12} | 6.088×10^{12} | 7.630×10^{11} |
| D_1 (kcal mol ⁻¹) | 11.50 | 21.98 | 24.13 | 23.50 | 25.87 |
| D_2 (K kcal mol ⁻¹) | 1.005×10^3 | 1.757×10^3 | 2.246×10^3 | 2.138×10^3 | 2.326×10^3 |
| RMSR | 0.051 | 0.159 | 0.122 | 0.099 | 0.082 |
| Model 3 $k = A \left(\frac{T}{300} \right)^n e^{-\frac{E(T+T_0)}{R(T^2+T_0^2)}}$ | | | | | |
| A (s ⁻¹) | 1.201×10^{11} | 2.533×10^{11} | 9.236×10^{11} | 1.163×10^{11} | 1.635×10^9 |
| n | 0.479 | 0.477 | 0.237 | 1.038 | 1.963 |
| E (kcal mol ⁻¹) | 6.511 | 13.13 | 14.77 | 13.31 | 13.53 |
| T_0 (K) | 254.2 | 235.85 | 278.1 | 268.0 | 259.7 |
| RMSR | 0.060 | 0.071 | 0.068 | 0.015 | 0.010 |

^a From CVT/SCT rate constants with harmonic-oscillator approximation for R1–R4 and hindered-rotor approximation for torsion modes for R5 with other modes treated as harmonic oscillators.

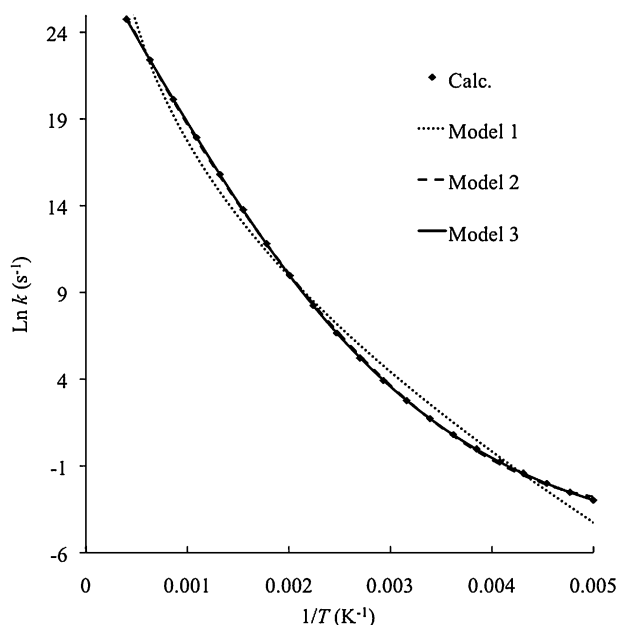


Fig. 6 Plot of the calculated CVT/SCT $\ln k$ vs. $1/T$ for reaction R2 along with rate constants obtained by fitted Model 1, Model 2, and Model 3. The harmonic-oscillator approximation was used for treating all vibrations, and the M08-SO/cc-pVTZ+ density functional approximation was used.

determine all parameters in Model 3, although it doesn't have the correct low-temperature asymptotics. We recommend Model 3 for fitting since it gives very small fitting errors for the reactions studied in this work and has the correct low-temperature asymptotics, which is very important to generate accurate rate constants at any temperature within the range that is used in the fitting and to extrapolate the rate constants beyond the temperature range that used in the fitting. We note that some reactions might have a temperature dependence of the activation energy like eqn (5), and others might have a temperature dependence like eqn (7). A key benefit of Model 3 is that it is general enough to provide a good fit in either case. If there is not enough data over a wide enough temperature range to justify four fitting parameters one can arbitrarily fix n or T_0 (for example, setting one or the other to zero) and use it as a three-parameter function. Note that one can also obtain the correct limit at 0 K by using $(T + T_0)^{-1}$ instead of $(T + T_0)(T^2 + T_0^2)^{-1}$ in eqn (8), but the form in eqn (8) seems to have a more physical behavior at low T .

We don't recommend Model 3 or any other model to be used for extrapolation to temperatures that are far away from the temperature range used in the fitting.

4. Concluding remarks

In this work, we present a set of best estimates of barrier heights and reaction energies of five intramolecular hydrogen-transfer isomerizations of butoxyl radicals. Based on assessment against our benchmark data, the M08-SO density functional is used for potential energy surface calculations in direct dynamics. Rate constants of five isomerization reactions were predicted for temperatures from 200 K to 2500 K using

canonical variational theory with multidimensional tunneling contributions. This study shows the importance of performing rate calculations with proper accounting for tunneling and torsional anharmonicity. We also proposed two new models for use in fitting rate constants over wide ranges of temperature.

Acknowledgements

This work was supported in part by the U.S. Department of Energy, Office of Science, Office of Basic Energy Sciences, as part of the Combustion Energy Frontier Research Center under Award Number DE-SC0001198. Part of the computation performed as part of a Computational Grand Challenge grant at the Molecular Science Computing Facility (MSCF) in the William R. Wiley Environmental Molecular Sciences Laboratory, a national scientific user facility sponsored by the U.S. Department of Energy's Office of Biological and Environmental Research and located at the Pacific Northwest National Laboratory, operated for the Department of Energy by Battelle.

References

- 1 ButylFuel LLC, <http://www.butanol.com/>.
- 2 J. T. Moss, A. M. Berkowitz, M. A. Oehlschlaeger, J. Biet, V. Warth, P.-A. Glaude and F. Battin-Leclerc, *J. Phys. Chem. A*, 2008, **112**, 10843.
- 3 P. Dagaut and C. Togbè, *Fuel*, 2008, **87**, 3313.
- 4 S. M. Sarathy, M. J. Thomson, C. Togbè, P. Dagaut, F. Halter and C. Mounaim-Rousselle, *Combust. Flame*, 2009, **156**, 852.
- 5 P. Dagaut and C. Togbè, *Energy Fuels*, 2009, **23**, 3527.
- 6 X. Gu, Z. Huang, Q. Li and C. Tang, *Energy Fuels*, 2009, **23**, 4900.
- 7 A. Heiss and K. Sahetchian, *Int. J. Chem. Kinet.*, 1996, **28**, 531.
- 8 R. Mereau, M. T. Rayez, F. Caralp and J. C. Rayez, *Phys. Chem. Chem. Phys.*, 2000, **2**, 1919.
- 9 G. Lendvay and B. Viskolcz, *J. Phys. Chem. A*, 1998, **102**, 10777.
- 10 H. Somnitz, *Phys. Chem. Chem. Phys.*, 2008, **10**, 965.
- 11 C. F. Melius, *Springer-Verlag DFVLR Lecture Notes*, Springer-Verlag, Berlin, 1990.
- 12 L. A. Curtiss, K. Raghavachari, G. W. Trucks and J. A. Pople, *J. Chem. Phys.*, 1991, **94**, 7221.
- 13 L. A. Curtiss, K. Raghavachari, P. C. Redfern, V. Rassolov and J. A. Pople, *J. Chem. Phys.*, 1998, **109**, 7764.
- 14 W. Kohn, A. D. Becke and R. G. Parr, *J. Phys. Chem.*, 1996, **100**, 12974.
- 15 J. Zheng, Y. Zhao and D. G. Truhlar, *J. Chem. Theory Comput.*, 2009, **5**, 808.
- 16 K. Raghavachari, G. W. Trucks, J. A. Pople and M. Head-Gordon, *Chem. Phys. Lett.*, 1989, **157**, 479.
- 17 K. A. Peterson, D. E. Woon and T. H. Dunning, Jr., *J. Chem. Phys.*, 1994, **100**, 7410.
- 18 I. S. Y. Wang and M. Karplus, *J. Am. Chem. Soc.*, 1973, **95**, 8160.
- 19 D. G. Truhlar, J. W. Duff, N. C. Blais, J. C. Tully and B. C. Garrett, *J. Chem. Phys.*, 1982, **77**, 764.
- 20 S. M. Colwell, *Theor. Chim. Acta*, 1988, **74**, 123.
- 21 K. K. Baldridge, M. S. Gordon, R. Steckler and D. G. Truhlar, *J. Phys. Chem.*, 1989, **93**, 5107.
- 22 D. G. Truhlar and M. S. Gordon, *Science*, 1990, **249**, 491.
- 23 Y.-P. Liu, G. C. Lynch, T. N. Truong, D.-h. Lu, D. G. Truhlar and B. C. Garrett, *J. Am. Chem. Soc.*, 1993, **115**, 2408.
- 24 Y.-P. Liu, D.-h. Lu, A. Gonzalez-Lafont, D. G. Truhlar and B. C. Garrett, *J. Am. Chem. Soc.*, 1993, **115**, 7806.
- 25 M. Page, *Comput. Phys. Commun.*, 1994, **84**, 115.
- 26 P. Cassanelli, D. Johnson and R. A. Cox, *Phys. Chem. Chem. Phys.*, 2005, **7**, 3702.
- 27 B. C. Garrett and D. G. Truhlar, *J. Chem. Phys.*, 1979, **70**, 1593.
- 28 D. G. Truhlar and B. C. Garrett, *Acc. Chem. Res.*, 1980, **13**, 440.

- 29 D. G. Truhlar, A. D. Isaacson, R. T. Skodje and B. C. Garrett, *J. Phys. Chem.*, 1982, **86**, 2252.
- 30 D. G. Truhlar and B. C. Garrett, *Annu. Rev. Phys. Chem.*, 1984, **35**, 159.
- 31 A. Fernandez-Ramos, B. A. Ellingson, B. C. Garrett and D. G. Truhlar, in *Reviews in Computational Chemistry*, ed. T. R. Cundari and K. B. Lipkowitz, Wiley-VCH, Hoboken, NJ, 2007, vol. 23, p. 125.
- 32 D.-h. Lu, T. N. Truong, V. S. Melissas, G. C. Lynch, Y.-P. Liu, B. C. Garrett, R. Steckler, A. D. Isaacson, S. N. Rai, G. C. Hancock, J. G. Lauderdale, T. Joseph and D. G. Truhlar, *Comput. Phys. Commun.*, 1992, **71**, 235.
- 33 T. H. Dunning, Jr., *J. Chem. Phys.*, 1989, **90**, 1007.
- 34 R. A. Kendall, T. H. Dunning and R. J. Harrison, *J. Chem. Phys.*, 1992, **96**, 6796.
- 35 J. M. L. Martin and P. R. Taylor, *Chem. Phys. Lett.*, 1994, **225**, 473.
- 36 J. M. L. Martin, *Chem. Phys. Lett.*, 1995, **242**, 343.
- 37 R. D. Cowan and D. C. Griffin, *J. Opt. Soc. Am.*, 1976, **66**, 1010.
- 38 R. L. Martin, *J. Phys. Chem.*, 1983, **87**, 750.
- 39 R. J. Gdanitz and R. Ahlrichs, *Chem. Phys. Lett.*, 1988, **143**, 413.
- 40 J. M. L. Martin and G. de Oliveira, *J. Chem. Phys.*, 1999, **111**, 1843.
- 41 Y. Zhao and D. G. Truhlar, *Theor. Chem. Acc.*, 2008, **120**, 215.
- 42 B. J. Lynch and D. G. Truhlar, *J. Phys. Chem. A*, 2003, **107**, 3898.
- 43 T. Clark, J. Chandrasekhar, G. W. Spitznagel and P. V. Schleyer, *J. Comput. Chem.*, 1983, **4**, 294.
- 44 H.-J. Werner, P. J. Knowles, R. Lindh, F. R. Manby, M. Schutz, P. Celani, T. Korona, A. Mitrushenkov, G. Rauhut, T. B. Adler, R. D. Amos, A. Bernhardsson, A. Berning, D. L. Cooper, M. J. O. Deegan, A. J. Dobbyn, F. Eckert, E. Goll, C. Hampel, G. Hetzer, T. Hrenar, G. Knizia, C. Koepl, Y. Liu, A. W. Lloyd, R. A. Mata, A. J. May, S. J. McNicholas, W. Meyer, M. E. Mura, A. Nicklass, P. Palmieri, K. Pfueger, R. Pitzer, M. Reiher, U. Schumann, H. Stoll, A. J. Stone, R. Tarroni, T. Thorsteinsson, M. Wang and A. Wolf, *MOLPRO*, 2008.1, 2008.
- 45 A. D. Becke, *Phys. Rev. A: At., Mol., Opt. Phys.*, 1988, **38**, 3098.
- 46 C. T. Lee, W. T. Yang and R. G. Parr, *Phys. Rev. B: Condens. Matter*, 1988, **37**, 785.
- 47 P. J. Stephens, F. J. Devlin, C. F. Chabalowski and M. J. Frisch, *J. Phys. Chem.*, 1994, **98**, 11623.
- 48 Y. Zhao, B. J. Lynch and D. G. Truhlar, *J. Phys. Chem. A*, 2004, **108**, 2715.
- 49 A. D. Becke, *J. Chem. Phys.*, 1996, **104**, 1040.
- 50 A. D. Boese and J. M. L. Martin, *J. Chem. Phys.*, 2004, **121**, 3405.
- 51 Y. Zhao, N. E. Schultz and D. G. Truhlar, *J. Chem. Phys.*, 2005, **123**, 161103.
- 52 Y. Zhao and D. G. Truhlar, *J. Chem. Theory Comput.*, 2008, **4**, 1849.
- 53 B. J. Lynch, P. L. Fast, M. Harris and D. G. Truhlar, *J. Phys. Chem. A*, 2000, **104**, 4811.
- 54 Y. Zhao and D. G. Truhlar, *J. Phys. Chem. A*, 2004, **108**, 6908.
- 55 C. Adamo and V. Barone, *J. Chem. Phys.*, 1998, **108**, 664.
- 56 Y. Zhao and D. G. Truhlar, *J. Phys. Chem. A*, 2005, **109**, 5656.
- 57 J.-D. Chai and M. Head-Gordon, *J. Chem. Phys.*, 2008, **128**, 084106.
- 58 J.-D. Chai and M. Head-Gordon, *Phys. Chem. Chem. Phys.*, 2008, **10**, 6615.
- 59 D. E. Woon and T. H. Dunning, *J. Chem. Phys.*, 1993, **98**, 1358.
- 60 E. Papajak, H. Leverentz, J. Zheng and G. T. Donald, *J. Chem. Theory Comput.*, 2009, **5**, 1197.
- 61 M. J. Frisch, G. W. Trucks, H. B. Schlegel, G. E. Scuseria, M. A. Robb, J. R. Cheeseman, V. G. Zakrzewski, J. A. Montgomery, R. E. Stratmann, J. C. Burant, S. Dapprich, J. M. Millam, A. D. Daniels, K. N. Kudin, M. C. Strain, O. Farkas, J. Tomasi, V. Barone, M. Cossi, R. Cammi, B. Mennucci, C. Pomelli, C. Adamo, S. Clifford, J. Ochterski, G. A. Petersson, P. Y. Ayala, Q. Cui, K. Morokuma, D. K. Malick, A. D. Rabuck, K. Raghavachari, J. B. Foresman, J. Cioslowski, J. V. Ortiz, A. G. Baboul, B. B. Stefanov, G. Liu, A. Liashenko, P. Piskorz, I. Komaromi, R. Gomperts, R. L. Martin, D. J. Fox, T. Keith, M. A. Al-Laham, C. Y. Peng, A. Nanayakkara, M. Challacombe, P. M. W. Gill, B. G. Johnson, W. Chen, M. W. Wong, J. L. Andres, C. Gonzalez, M. Head-Gordon, E. S. Replogle and J. A. Pople, *GAUSSIAN03*, Gaussian, Inc., Pittsburgh, PA, Revision E.01, 2003.
- 62 Y. Zhao and D. G. Truhlar, *MN-GFM: Minnesota Gaussian Functional Module*, University of Minnesota, Minneapolis, version 4.1, 2007.
- 63 M. J. Frisch, G. W. Trucks, H. B. Schlegel, G. E. Scuseria, M. A. Robb, J. R. Cheeseman, G. Scalmani, V. Barone, B. Mennucci, G. A. Petersson, H. Nakatsuji, M. Caricato, X. Li, H. P. Hratchian, A. F. Izmaylov, J. Bloino, G. Zheng, J. L. Sonnenberg, M. Hada, M. Ehara, K. Toyota, R. Fukuda, J. Hasegawa, M. Ishida, T. Nakajima, Y. Honda, O. Kitao, H. Nakai, T. Vreven, J. A. Montgomery Jr, J. E. Peralta, F. Ogliaro, M. Bearpark, J. J. Heyd, E. Brothers, K. N. Kudin, V. N. Staroverov, R. Kobayashi, J. Normand, K. Raghavachari, A. Rendell, J. C. Burant, S. S. Iyengar, J. Tomasi, M. Cossi, N. Rega, J. M. Millam, M. Klene, J. E. Knox, J. B. Cross, V. Bakken, C. Adamo, J. Jaramillo, R. E. Gomperts, O. Stratmann, A. J. Yazyev, R. Austin, C. Cammi, J. W. Pomelli, R. Ochterski, R. L. Martin, K. Morokuma, V. G. Zakrzewski, G. A. Voth, P. Salvador, J. J. Dannenberg, S. Dapprich, A. D. Daniels, O. Farkas, J. B. Foresman, J. V. Ortiz, J. Cioslowski and D. J. Fox, *Gaussian 09*, Gaussian Inc., Wallingford, CT, Revision A.02, 2009.
- 64 K. S. Pitzer and W. D. Gwinn, *J. Chem. Phys.*, 1942, **10**, 428.
- 65 K. S. Pitzer, *J. Chem. Phys.*, 1946, **14**, 239.
- 66 D. G. Truhlar, *J. Comput. Chem.*, 1991, **12**, 266.
- 67 B. A. Ellingson, V. A. Lynch, S. L. Mielke and D. G. Truhlar, *J. Chem. Phys.*, 2006, **125**, 084305.
- 68 Y.-Y. Chuang and D. G. Truhlar, *J. Chem. Phys.*, 2000, **112**, 1221.
- 69 Y.-Y. Chuang and D. G. Truhlar, *J. Chem. Phys.*, 2006, **124**, 179903.
- 70 Y.-Y. Chuang and D. G. Truhlar, *J. Chem. Phys.*, 2004, **121**, 7036.
- 71 J. C. Corchado, E. L. Coitiño, Y.-Y. Chuang, P. L. Fast and D. G. Truhlar, *J. Phys. Chem. A*, 1998, **102**, 2424.
- 72 M. Page and J. W. McIver, Jr., *J. Chem. Phys.*, 1988, **88**, 922.
- 73 C. F. Jackels, Z. Gu and D. G. Truhlar, *J. Chem. Phys.*, 1995, **102**, 3188.
- 74 Y.-Y. Chuang and D. G. Truhlar, *J. Phys. Chem. A*, 1998, **102**, 242.
- 75 P. L. Fast, J. Corchado, M. L. Sanchez and D. G. Truhlar, *J. Phys. Chem. A*, 1999, **103**, 3139.
- 76 J. M. L. Martin, *J. Chem. Phys.*, 1992, **97**, 5012.
- 77 J. Zheng, S. Zhang, J. C. Corchado, Y.-Y. Chuang, E. L. Coitiño, B. A. Ellingson and D. G. Truhlar, *GAUSSRATE*, University of Minnesota, Minneapolis, 2008.
- 78 J. Zheng, S. Zhang, B. J. Lynch, J. C. Corchado, Y.-Y. Chuang, P. L. Fast, W.-P. Hu, Y.-P. Liu, G. C. Lynch, K. A. Nguyen, C. F. Jackels, A. F. Ramos, B. A. Ellingson, V. S. Melissas, J. Villà, I. Rossi, E. L. Coitino, J. Pu, T. V. Albu, R. Steckler, B. C. Garrett, A. D. Isaacson and D. G. Truhlar, *POLYRATE*, University of Minnesota, Minneapolis, 2008.
- 79 D. G. Truhlar, *J. Chem. Educ.*, 1978, **55**, 309.
- 80 D. Gruzman, A. Karton and J. M. L. Martin, *J. Phys. Chem. A*, 2009, **113**, 11974.
- 81 D. G. Truhlar and A. Kuppermann, *J. Am. Chem. Soc.*, 1971, **93**, 1840.
- 82 T. C. Allison and D. G. Truhlar, in *Modern Methods for Multidimensional Dynamics Computations in Chemistry*, ed. D. L. Thompson, World Scientific, Singapore, 1998, p. 618.
- 83 S. E. Wonchoba, W.-P. Hu and D. G. Truhlar, *Phys. Rev. B: Condens. Matter*, 1995, **51**, 9985.
- 84 P. S. Zuev, R. S. Sheridan, T. V. Albu, D. G. Truhlar, D. A. Hrovat and W. T. Borden, *Science*, 2003, **299**, 867.